Chemical Science

ROYAL SOCIETY OF CHEMISTRY

EDGE ARTICLE

View Article Online
View Journal | View Issue

Cite this: *Chem. Sci.*, 2024, **15**, 11500

All publication charges for this article have been paid for by the Royal Society of Chemistry

Received 11th March 2024
Accepted 18th June 2024

DOI: 10.1039/d4sc01650e

rsc.li/chemical-science

Crystalline organic monoliths with bicontinuous porosity†

Naoto Matsumoto,[a] Sakura Nakagawa,[a] Kei Morisato,[b] Kazuyoshi Kanamori,[be] Kazuki Nakanishi[cd] and Nobuhiro Yanai[*afg]

Organic crystals are a promising class of materials for various optical applications. However, it has been challenging to make macroscopic organic crystals with bicontinuous porosity that are applicable to flow chemistry. In this study, a new class of porous materials, cm-scale crystalline organic monoliths (COMs) with bicontinuous porosity, are synthesized by replicating the porous structure of silica monolith templates. The COMs composed of *p*-terphenyl can take up more than 30 wt% of an aqueous solution, and the photophysical properties of the *p*-terphenyl crystals are well maintained in the COMs. The relatively high surface area of the COMs can be exploited for efficient Dexter energy transfer from triplet sensitizers on the pore surface. The resulting triplet excitons in the COMs encounter and annihilate, generating upconverted UV emission. The COMs would open a new avenue toward applications of organic crystals in flow photoreaction systems.

Introduction

Organic crystals have attracted much attention for their intriguing luminescence functions such as solid-state fluorescence,[1,2] photon upconversion,[3–5] room-temperature phosphorescence,[6–9] photochromism,[10] and optical waveguides.[11–14] While the size of organic crystals is typically in the range of μm to mm, macroscopic organic crystals on the cm-scale have also been exploited. Macroscopic crystals of polyaromatic hydrocarbons (PAHs) have been studied as organic scintillators.[15–18] Acene-doped PAH single crystals have also been used for microwave amplification by stimulated emission of radiation (MASER)[19–21] and dynamic nuclear polarization using photoexcited triplet electrons (triplet-DNP).[22–25] These bulk crystals can be prepared by melting the components and subsequent cooling. On the other hand, these bulk crystals have only been used in "dry" systems, and their limited surface area made it difficult to interact with molecules in solution.

Here, we propose a new class of porous materials, crystalline organic monoliths (COMs). Monoliths with bicontinuous porous structures composed of silica and organic polymers have been used as adsorbents, supports, and chromatographic columns.[26–34] While some photofunctional titania monoliths have been developed,[35–37] examples of photofunctional organic monoliths have been limited.[38] If bicontinuous porous monoliths can be created with organic crystals, the long exciton diffusion length in organic crystals would enable excitons to reach the pore surface to be utilized.[39,40] This novel design of monoliths allows conventional bulk organic crystals to interact with molecules in solution effectively. We synthesized COMs using a template replication method. First, a melt of *p*-terphenyl (TP), a model compound, was introduced into the pores of template silica monoliths. A base treatment removed the template, leaving TP-based COMs (TP-COMs) with bicontinuous pore structures. The pore surface of the TP-COMs could be utilized for Dexter energy transfer. Upon visible light irradiation, surface-mediated triplet energy transfer from sensitizer molecules to the TP-COMs and subsequent triplet–triplet annihilation (TTA) resulted in upconverted UV emission from the TP-COMs. The visible-to-UV photon upconversion of the COM containing aqueous solutions shows their promising potential for applications in flow photochemistry.

Results and discussion

Synthesis of TP-based COMs (TP-COMs)

We used silica monoliths as templates because they can be easily removed by hydrolysis without dissolving organic crystals. Silica monolith is a monolithic gel with a hierarchical

[a]*Department of Applied Chemistry, Graduate School of Engineering, Kyushu University, 744 Moto-oka, Nishi-ku, Fukuoka 819-0395, Japan. E-mail: Yanai@mail.cstm.kyushu-u.ac.jp*

[b]*Department of Chemistry, Graduate School of Science, Kyoto University, Kitashirakawa, Sakyo-ku, Kyoto 606-8502, Japan*

[c]*Institute of Materials and Systems for Sustainability, Nagoya University, Furo-cho, Chikusa-ku, Nagoya, Aichi 464-8601, Japan*

[d]*Institute for Integrated Cell-Material Sciences, Kyoto University, Yoshida, Sakyo-ku, Kyoto 606-8501, Japan*

[e]*PRESTO, JST, Honcho 4-1-8, Kawaguchi, Saitama 332-0012, Japan*

[f]*FOREST, JST, Honcho 4-1-8, Kawaguchi, Saitama 332-0012, Japan*

[g]*CREST, JST, Honcho 4-1-8, Kawaguchi, Saitama 332-0012, Japan*

† Electronic supplementary information (ESI) available. See DOI: https://doi.org/10.1039/d4sc01650e

porous structure, and the pore structure can be tuned using synthetic conditions.[27] Silica monoliths were synthesized following the previous report (Fig. 1a).[27] Urea and poly(ethylene glycol) (MW: ~10 000, PEG10 000) were dissolved in an aqueous acetic acid solution. After complete dissolution, tetramethoxysilane (TMOS) was added to the mixture and allowed to react in an ice bath. After stirring for 90 minutes, the resulting mixture was transferred to a water bath at 30 °C for gelation. The resulting gels were heated to 110 °C for 4 hours to modulate the mesoporous structure. After washing and drying, the resulting gels were calcined at 600 °C for 5 hours to yield white silica monoliths (Fig. 1c). Scanning electron microscopy (SEM)

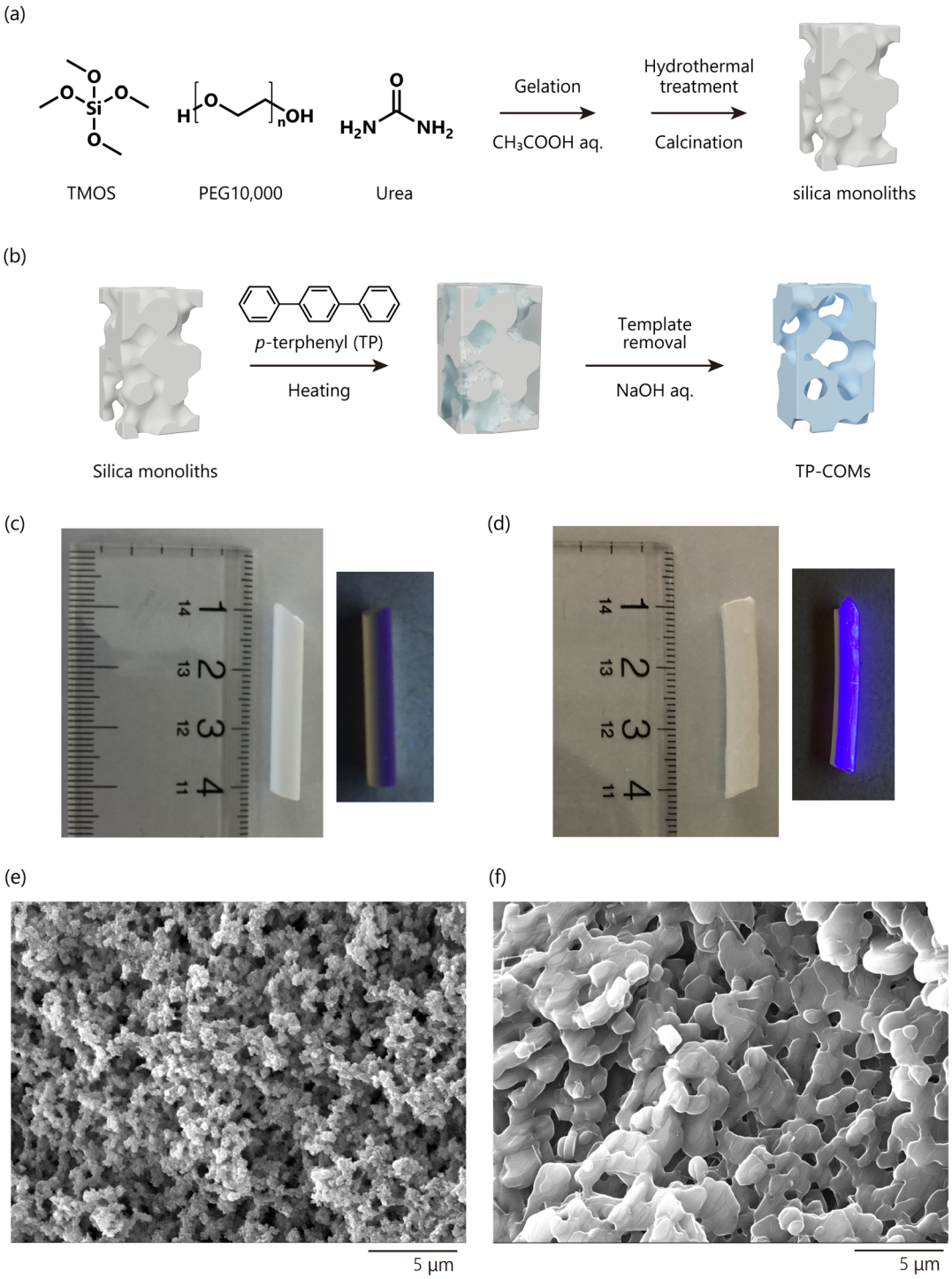

Fig. 1 (a) Synthetic scheme of silica monoliths. TMOS: tetramethoxysilane and PEG10 000: poly(ethylene glycol) mw: 10 000. (b) Synthetic scheme of TP-COMs. Photographs without (left) and with (right) UV light irradiation of (c) silica monoliths and (d) TP-COMs. (e) SEM images of silica monoliths and (f) TP-COMs.

images after calcination showed the formation of bicontinuous macroporous structures with an average silica width of 0.73 ± 0.04 μm and pore sizes ranging from 1.0 to 3.3 μm (Fig. 1e). In addition, N_2 adsorption analysis at 77 K showed that the Brunauer–Emmett–Teller (BET) surface area was 362 $m^2\ g^{-1}$, and the mesopore size estimated from the Barrett–Joyner–Halenda (BJH) method was about 15.6 nm (Fig. S1†). The formation of mesopores is typical of silica monoliths synthesized by this method, confirming the successful synthesis of silica monoliths. When exposed to water, the silica monoliths exhibited 79.2 wt% of water uptake according to the thermogravimetric analysis (TGA) curves (Fig. 2a). Considering the density of silica gel (0.7 g cm^{-3}) and water (1.0 g cm^{-3}), the volume ratio of pores in the silica monoliths was calculated to be 72.7 vol%.

The porous structure of silica monoliths has been transferred to organic crystals (Fig. 1b). In this work, *p*-terphenyl (TP) was chosen as a model compound to synthesize crystalline monoliths because TP has significant thermal stability and photoluminescence. A glass tube filled with the silica monoliths and TP powder was frame-sealed under reduced pressure. The sample was heated to 230 °C to introduce the molten TP into the pores of the silica monoliths. After cooling down to room temperature, excess TP was removed (see details in the ESI†). The resulting composite was immersed in a 1 M NaOH aqueous solution to dissolve the silica by hydrolysis. The resulting sample was washed with water and dried under reduced pressure to obtain TP-based crystalline organic monoliths (TP-COMs). While the original silica monoliths showed no luminescence under UV light irradiation (Fig. 1c), the obtained TP-COMs showed bright purple luminescence (Fig. 1d).

The introduction of TP into the silica pores and the removal of silica were tracked by TGA (Fig. 2b). The introduction of TP into the silica monoliths resulted in an 82.5% weight loss, which corresponds to 73.3 vol% of TP in silica monoliths (density of TP was estimated to be 1.2 g cm^{-3} based on the single crystal structure[41]). This value agrees well with the estimated porosity of water-filled silica monoliths (72.7 vol%), indicating that the pores of the silica monoliths were filled with TP. Furthermore, the TGA curve of TP-COMs reached 100% weight loss at around 230 °C, confirming the complete removal of the silica templates.

The porous structure of the TP-COMs was also investigated. SEM images of the TP-COMs showed a bicontinuous porous structure with an average size of pore walls and pore sizes of 3.0 ± 0.17 μm and 1.8 ± 0.14 μm, respectively, indicating the successful replication of the template silica monoliths (Fig. 1f). Since the pore surface of TP-COMs was too hydrophobic to take up water, an aqueous solution of 10 mM cetyltrimethylammonium bromide (CTAB) surfactant was introduced into the TP-COMs. The volume ratio of the aqueous solution in the TP-COM was estimated to be 32.8 vol% from the TGA curve (Fig. 2C). The volume ratio of TP to the silica monolith template (73.3 vol%) predicts the pore volume ratio of the TP-COMs to be 26.7 vol%. This predicted value is not far from the observed value (32.8 vol%), indicating the successful transfer of the porous structure from silica monoliths to TP-COMs. On the other hand, the N_2 adsorption analysis showed less than 1.0 $m^2\ g^{-1}$ of BET surface area, indicating that TP-COMs have a macroporous structure but are nonporous at the nanoscale (Fig. S1†). The current method successfully replicated the macropores but not the mesopores of the silica template, so further developments are needed to improve the surface area of the resulting COMs. The powder X-ray diffraction measurements supported the fact that the crystalline structure of TP is well preserved in the resulting TP-COMs (Fig. S3†). This simple melt crystallization and template removal method successfully synthesized the organic crystalline monoliths.

The morphology of the TP-COMs can be easily tuned by changing the porous structure of the silica monolith templates. By using different amounts of PEG10 000, the 3 types of silica monoliths were synthesized. Using these templates, corresponding porous structures of TP-COMs were successfully obtained (Fig. S4†). This result indicates that this method has excellent versatility in synthesizing COMs with different porous structures. The following demonstrations utilized TP-COMs synthesized with silica monolith using 575 mg of PEG10 000.

The optical properties of TP-COMs were evaluated. Although UV-vis absorption spectra could not be recorded due to the strong scattering, excitation and fluorescence spectra showed a similar spectral shape to TP powder (Fig. S5†). In addition, the TP powder shows a high fluorescence quantum yield (66.5%),

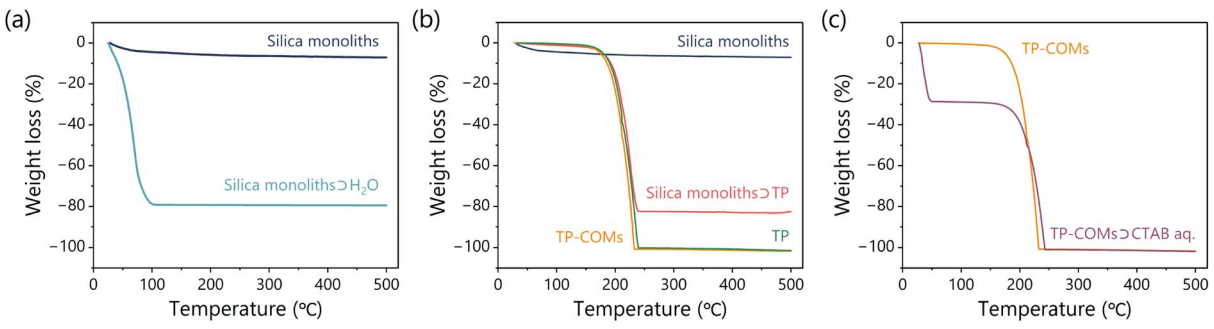

Fig. 2 TGA curves of (a) silica monoliths (black) and silica monoliths exposed to water (blue), (b) silica monoliths (black), composite of silica monoliths and TP (red), TP powder (green), and TP-COMs (orange), (c) TP-COMs (orange) and TP-COMs immersed in the 10 mM aqueous CTAB solution (purple). The same color data represent the same sample.

which is mostly preserved in the TP-COMs (57.0%). This indicates that TP-COMs can be a promising UV-emitting bulk material with high porosity.

Dexter energy transfer at the pore surface of COMs

The triplet Dexter energy transfer at the pore surface of the TP-COMs has been investigated. The organic crystals of π-conjugated compounds with high porosity have the potential to harvest and convert light energy for various photochemical reactions. Here, we used the TP-COMs as triplet energy acceptors to demonstrate photon upconversion based on triplet–triplet annihilation (TTA-UC). As a triplet sensitizer, we chose $Ir(ppy)_3$, which has a suitable T_1 energy level ($T_1 = 2.48$ eV)[42] for efficient triplet energy transfer to TP crystals ($T_1 = 2.15$ eV).[43]

Dexter energy transfer requires close contact between $Ir(ppy)_3$ and TP molecules. Since TP is soluble in common organic solvents, the monolithic structure of TP-COMs is easily lost by organic solvents. On the other hand, hydrophobic $Ir(ppy)_3$ is not soluble in water. To overcome these problems, we used an aqueous micelle solution to modify $Ir(ppy)_3$ on the pore surface of TP-COMs (Fig. 3a). The incorporation of $Ir(ppy)_3$ into the micelle allowed $Ir(ppy)_3$ to dissolve in water. The use of surfactants also allowed the aqueous solution to be introduced into the highly hydrophobic pores by reducing the surface tension. A THF solution of $Ir(ppy)_3$ was added to the aqueous solution of the surfactant CTAB, and stirred overnight, resulting in the $Ir(ppy)_3$-dispersed micelle solution. After syringe filtration, the formation of $Ir(ppy)_3$-dispersed micelles was confirmed by dynamic light scattering (DLS) and zeta potential measurements. An average micelle size of 3.21 ± 0.43 nm (Fig. 3b) and a zeta potential of +60.7 ± 1.5 mV were observed, indicating the formation of the CTAB micelles. Absorption and photoluminescence spectra of the micelle solution confirmed the inclusion of $Ir(ppy)_3$ (Fig. 3c), and the concentration of $Ir(ppy)_3$ was roughly estimated to be 9.3 μM from the absorbance of the aqueous micelle and the molar absorption coefficient in CH_2Cl_2 ($\varepsilon_{377} = 12\,000\ M^{-1}\ cm^{-1}$) (Fig. S6†).[44]

To modify the macropore surface of the TP-COMs with $Ir(ppy)_3$, the TP-COMs were immersed in the $Ir(ppy)_3$ micellar solution. After 2 hours of immersion, the resulting sample was washed with water and dried under reduced pressure. The macropore structure of the TP-COMs was well preserved after the $Ir(ppy)_3$ modification (Fig. S7†). The modification of $Ir(ppy)_3$ was confirmed by photoluminescence spectra (Fig. S8†). Notably, the similar photoluminescence spectra of $Ir(ppy)_3$ on the TP-COMs compared to those in the toluene solution indicated the good dispersibility of $Ir(ppy)_3$ on the surface of TP-COMs (Fig. S8†). On the other hand, the amount of $Ir(ppy)_3$ on the surface of the TP-COMs could not be determined due to its low concentration.

The TET process was evaluated by monitoring the change in the photoluminescence lifetime of $Ir(ppy)_3$ (Fig. 4a). The photoluminescence lifetime of $Ir(ppy)_3$ on the pore surface of the TP-COMs became significantly shorter than that in the toluene solution (Fig. 4b). The photoluminescence decay of $Ir(ppy)_3$ on the TP-COMs could be fitted with a biexponential function. The mean photoluminescence lifetime was 0.38 μs (Fig. 4b, Table S1†). The TET efficiency was calculated using the following equation:

$$\Phi_{ET} = 1 - \tau/\tau_0$$

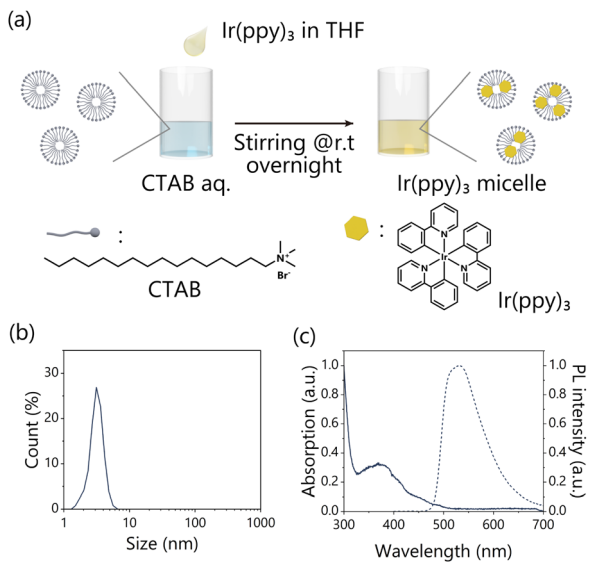

Fig. 3 (a) Schematic representation of $Ir(ppy)_3$ micelle preparation and chemical structures of CTAB and $Ir(ppy)_3$. (b) DLS profile of $Ir(ppy)_3$ micelles. (c) UV-vis absorption (solid line) and photoluminescence (dotted line) spectra of $Ir(ppy)_3$ micelles in water.

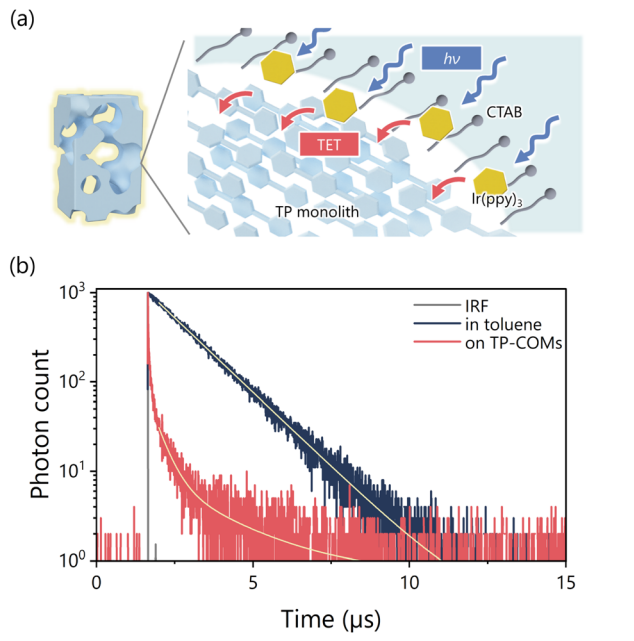

Fig. 4 (a) Schematic representation of triplet Dexter energy transfer on the macropore surface of TP-COMs. (b) Photoluminescence decays and fitted lines (yellow) of $Ir(ppy)_3$ in toluene (black) and on the surface of TP-COMs (red). The instrument response function (IRF) is shown in the gray line.

where Φ_{ET} is the energy transfer efficiency, τ is the average photoluminescence lifetime of $Ir(ppy)_3$ on the surface of the TP-COMs, and τ_0 is the lifetime of $Ir(ppy)_3$ in toluene (1.30 μs). The Φ_{ET} was estimated to be 70.6%, demonstrating efficient Dexter energy transfer at the pore surface of the TP-COMs.

TTA-UC of $Ir(ppy)_3$-modified TP-COMs

Finally, the TTA-UC properties of $Ir(ppy)_3$ modified TP-COMs were evaluated. TTA-UC is one of the photon upconversion methods that can generate a higher energy photon from two lower energy photons.[45–58] The photo-excited sensitizer undergoes intersystem crossing (ISC) to the triplet state. The triplet energy of the sensitizer is then transferred to the emitter. When two triplets of the emitter encounter and annihilate, the upconverted singlet state of the emitter is generated (Fig. 5a). TTA-UC is promising because it can work at low excitation light intensity and yield high quantum efficiency, which is expected for various applications in energy and biology disciplines.[59–64]

The TTA-UC measurements were performed under an Ar atmosphere for $Ir(ppy)_3$ modified TP-COMs. Irradiation with a 445 nm continuous wave (CW) blue laser resulted in UC emission in the UV region with a peak top at 372 nm (Fig. 5b). The μs scale of the upconversion photoluminescence (UCPL) decay indicated that the triplet states were involved, and the triplet lifetime was estimated to be 133 μs (Fig. S9†). No UCPL was observed when the TP-COMs without $Ir(ppy)_3$ were excited using the 445 nm laser, supporting the sensitized TTA-UC mechanism. The TTA-UC efficiency could not be determined due to the low absorption of $Ir(ppy)_3$ on the surface of the TP-COMs and the intense light scattering of the TP-COMs. Interestingly, no UCPL was detected by photoexcitation of $Ir(ppy)_3$-doped TP powder prepared by melting and cooling $Ir(ppy)_3$-modified TP-COMs. This indicates that when $Ir(ppy)_3$ is uniformly dispersed throughout the TP powder, almost no TTA is observed due to the low concentration of $Ir(ppy)_3$ and, thus, the low concentration of triplet excitons. On the other hand, by selectively modifying $Ir(ppy)_3$ on the pore surface of TP-COMs, the local triplet density increases and TTA is effectively induced. This means that excitons can accumulate near the pore surface of the COMs and are expected to be applied to chemical reactions involving energy transfer and electron transfer using upconverted energy.

At low excitation intensities, TTA-UC behaves as a two-photon process because triplet deactivation occurs faster than TTA, but as the excitation light intensity is increased, triplet consumption by TTA becomes dominant, and the process behaves as a pseudo-one-photon process.[65–67] The threshold excitation intensity, I_{th}, is the point at which this quadratic to linear transition occurs and is estimated from the intersection of the fitting lines in the double logarithmic plot of UC emission intensity *versus* excitation light intensity (Fig. 6). I_{th} is a key parameter for evaluating TTA-UC because approximately half of the maximum UC efficiency of the system is obtained at I_{th}. The UC emission intensity at 372 nm of the $Ir(ppy)_3$-modified TP-COMs showed the expected quadratic-to-linear transition and a relatively low I_{th} of 750 mW cm^{-2} (Fig. 6). Notably, a similar I_{th} value of 1040 mW cm^{-2} was observed for the $Ir(ppy)_3$-modified TP-COMs immersed in degassed water for 2 h (Fig. 6). This indicates that the leakage of $Ir(ppy)_3$ into water is suppressed and that the upconverted energy can be utilized under aqueous conditions. An important step toward the possible development of a flow photoreaction system based on upconverting monoliths with bicontinuous porous structures has been demonstrated.

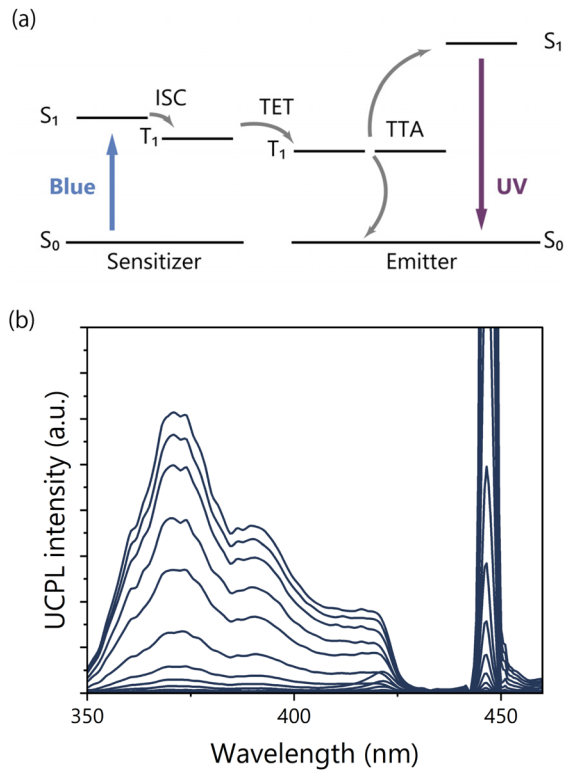

Fig. 5 (a) Schematic representation of TTA-UC. ISC: intersystem crossing, TET: triplet energy transfer, and TTA: triplet–triplet annihilation. (b) Upconversion photoluminescence (UCPL) spectra of $Ir(ppy)_3$-modified TP-COMs at different excitation intensities (λ_{ex} = 445 nm, 425 nm short pass filter).

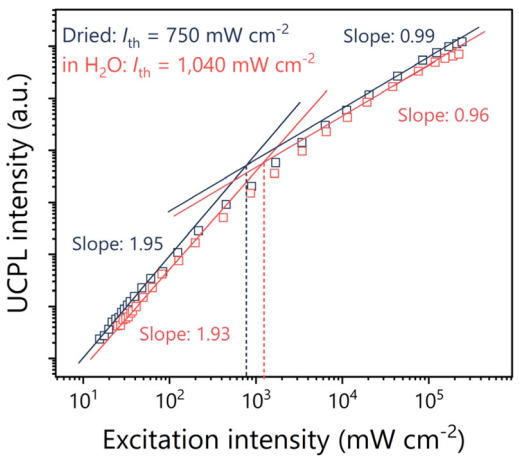

Fig. 6 Excitation intensity dependence of UCPL intensity at 372 nm of $Ir(ppy)_3$ modified TP-COMs under Ar (black) and in degassed water (red).

Conclusions

We have developed a method to impart bicontinuous porous structures to bulk organic crystals. Although examples of bicontinuous porous monoliths have been limited to amorphous materials, we have shown that the porous structure can be transferred to organic crystals using silica monoliths as templates. Furthermore, by modifying the monolith surface with a triplet sensitizer, we have succeeded in inducing highly efficient Dexter energy transfer and TTA-UC at relatively low excitation light intensities. The surface-mediated upconversion from visible light to UV light would lead to the flow of photochemical reaction systems. The method developed in this study is very simple and can be applied to various organic crystals. It will create a new class of materials called crystalline organic monoliths (COMs) with different optical and electronic functions.

Data availability

Data for this article are available at Zenodo at **https://zenodo.org/doi/10.5281/zenodo.11512823**.

Author contributions

N. Y. conceived the project. N. M. and S. N. carried out the experiments. K. M., K. K., and K. N. contributed to preparing the silica monolith templates. N. M. and N. Y. wrote the manuscript with the input of all co-authors.

Conflicts of interest

There are no conflicts to declare.

Acknowledgements

This work was partly supported by JST START (JPMJSF2303), JSPS KAKENHI (grant numbers JP23H00304, JP22K19051, and JP23KJ1715), the Murata Science Foundation, the Research Foundation for Opto-Science and Technology, the Kyushu University Platform of Inter-/Transdisciplinary Energy Research (Q-PIT) through its "Module-Research Program", and the Kyushu University Integrated Initiative for Designing Future Society.

Notes and references

1 H. Y. Zhang, Z. L. Zhang, K. Q. Ye, J. Y. Zhang and Y. Wang, *Adv. Mater.*, 2006, **18**, 2369–2372.
2 Q. Di, L. Li, X. Miao, L. Lan, X. Yu, B. Liu, Y. Yi, P. Naumov and H. Zhang, *Nat. Commun.*, 2022, **13**, 5280.
3 T. Ogawa, N. Yanai, S. Fujiwara, T.-Q. Nguyen and N. Kimizuka, *J. Mater. Chem. C*, 2018, **6**, 5609–5615.
4 C. D. Cruz, H. H. Choi, V. Podzorov, E. L. Chronister and C. J. Bardeen, *J. Phys. Chem. C*, 2018, **122**, 17632–17642.
5 R. Enomoto, M. Hoshi, H. Oyama, H. Agata, S. Kurokawa, H. Kuma, H. Uekusa and Y. Murakami, *Mater. Horiz.*, 2021, **8**, 3449–3456.
6 W. Z. Yuan, X. Y. Shen, H. Zhao, J. W. Y. Lam, L. Tang, P. Lu, C. Wang, Y. Liu, Z. Wang, Q. Zheng, J. Z. Sun, Y. Ma and B. Z. Tang, *J. Phys. Chem. C*, 2010, **114**, 6090–6099.
7 O. Bolton, K. Lee, H.-J. Kim, K. Y. Lin and J. Kim, *Nat. Chem.*, 2011, **3**, 205–210.
8 W. Zhao, Z. He and B. Z. Tang, *Nat. Rev. Mater.*, 2020, **5**, 869–885.
9 M. Singh, K. Liu, S. Qu, H. Ma, H. Shi, Z. An and W. Huang, *Adv. Opt. Mater.*, 2021, **9**, 2002197.
10 K. Amimoto and T. Kawato, *J. Photochem. Photobiol., C*, 2005, **6**, 207–226.
11 C. Zhang, Y. Yan, Y. S. Zhao and J. Yao, *Acc. Chem. Res.*, 2014, **47**, 3448–3458.
12 Y. Ma, Y. Zong, H. Yin, H. Lin, S. Chen and X.-D. Wang, *Adv. Opt. Mater.*, 2021, **9**, 2101481.
13 S. Wu, B. Zhou and D. Yan, *Adv. Opt. Mater.*, 2021, **9**, 2001768.
14 D. Tian and Y. Chen, *Adv. Opt. Mater.*, 2021, **9**, 2002264.
15 R. C. Sangster and J. W. Irvine Jr, *J. Chem. Phys.*, 1956, **24**, 670–715.
16 F. D. Brooks, *Nucl. Instrum. Methods*, 1979, **162**, 477–505.
17 S. V. Budakovsky, N. Z. Galunov, N. L. Karavaeva, J. K. Kim, Y. K. Kim, O. A. Tarasenko and E. V. Martynenko, *IEEE Trans. Nucl. Sci.*, 2007, **54**, 2734–2740.
18 N. Galunov, D. Gryn, N. Karavaeva, I. Khromiuk, I. Lazarev, O. Navozenko, A. Naumenko, O. Tarasenko and V. Yashchuk, *J. Lumin.*, 2020, **226**, 117477.
19 M. Oxborrow, J. D. Breeze and N. M. Alford, *Nature*, 2012, **488**, 353–356.
20 Q. Ai, P. Chen, Y. Feng and Y. Xu, *Cryst. Growth Des.*, 2017, **17**, 2473–2477.
21 S. Cui, Y. Liu, G. Li, Q. Han, C. Ge, L. Zhang, Q. Guo, X. Ye and X. Tao, *Cryst. Growth Des.*, 2020, **20**, 783–792.
22 A. Henstra, T.-S. Lin, J. Schmidt and W. T. Wenckebach, *Chem. Phys. Lett.*, 1990, **165**, 6–10.
23 M. Iinuma, Y. Takahashi, I. Shaké, M. Oda, H. M. Shimizu, A. Masaike and T. Yabuzaki, *J. Phys. Soc. Jpn.*, 2005, **74**, 2622–2630.
24 K. Tateishi, M. Negoro, S. Nishida, A. Kagawa, Y. Morita and M. Kitagawa, *Proc. Natl. Acad. Sci. U. S. A.*, 2014, **111**, 7527–7530.
25 T. R. Eichhorn, A. J. Parker, F. Josten, C. Müller, J. Scheuer, J. M. Steiner, M. Gierse, J. Handwerker, M. Keim, S. Lucas, M. U. Qureshi, A. Marshall, A. Salhov, Y. Quan, J. Binder, K. D. Jahnke, P. Neumann, S. Knecht, J. W. Blanchard, M. B. Plenio, F. Jelezko, L. Emsley, C. C. Vassiliou, P. Hautle and I. Schwartz, *J. Am. Chem. Soc.*, 2022, **144**, 2511–2519.
26 E. C. Peters, F. Svec and J. M. J. Fréchet, *Adv. Mater.*, 1999, **11**, 1169–1181.
27 K. Nakanishi, H. Shikata, N. Ishizuka, N. Koheiya and N. Soga, *J. High Resolut. Chromatogr.*, 2000, **23**, 106–110.
28 J. O. Krause, S. Lubbad, O. Nuyken and M. R. Buchmeiser, *Adv. Synth. Catal.*, 2003, **345**, 996–1004.

29 K. Cabrera, *J. Sep. Sci.*, 2004, **27**, 843–852.
30 F. Svec, *J. Sep. Sci.*, 2004, **27**, 747–766.
31 K. Nakanishi and N. Tanaka, *Acc. Chem. Res.*, 2007, **40**, 863–873.
32 A. Sachse, A. Galarneau, F. Fajula, F. Di Renzo, P. Creux and B. Coq, *Microporous Mesoporous Mater.*, 2011, **140**, 58–68.
33 R. Porta, M. Benaglia and A. Puglisi, *Org. Process Res. Dev.*, 2016, **20**, 2–25.
34 C.-H. Pélisson, T. Nakanishi, Y. Zhu, K. Morisato, T. Kamei, A. Maeno, H. Kaji, S. Muroyama, M. Tafu, K. Kanamori, T. Shimada and K. Nakanishi, *ACS Appl. Mater. Interfaces*, 2017, **9**, 406–412.
35 X. Fan, H. Fei, D. H. Demaree, D. P. Brennan, J. M. St. John and S. R. J. Oliver, *Langmuir*, 2009, **25**, 5835–5839.
36 O. Ruzimuradov, S. Nurmanov, M. Hojamberdiev, R. M. Prasad, A. Gurlo, J. Broetz, K. Nakanishi and R. Riedel, *J. Eur. Ceram. Soc.*, 2014, **34**, 809–816.
37 N. M. Nursam, X. Wang, J. Z. Y. Tan and R. A. Caruso, *ACS Appl. Mater. Interfaces*, 2016, **8**, 17194–17204.
38 S. Ghasimi, S. Prescher, Z. J. Wang, K. Landfester, J. Yuan and K. A. I. Zhang, *Angew. Chem., Int. Ed.*, 2015, **54**, 14549–14553.
39 G. M. Akselrod, P. B. Deotare, N. J. Thompson, J. Lee, W. A. Tisdale, M. A. Baldo, V. M. Menon and V. Bulović, *Nat. Commun.*, 2014, **5**, 3646.
40 O. V. Mikhnenko, P. W. M. Blom and T.-Q. Nguyen, *Energy Environ. Sci.*, 2015, **8**, 1867–1888.
41 H. M. Rietveld, E. N. Maslen and C. J. B. Clews, *Acta Crystallogr., Sect. B: Struct. Sci., Cryst. Eng. Mater.*, 1970, **26**, 693–706.
42 W. Zhao and F. N. Castellano, *J. Phys. Chem. A*, 2006, **110**, 11440–11445.
43 D. M. Niedzwiedzki, D. Mulrow and L. G. Sobotka, *J. Phys. Chem. A*, 2022, **126**, 5273–5282.
44 A. B. Tamayo, B. D. Alleyne, P. I. Djurovich, S. Lamansky, I. Tsyba, N. N. Ho, R. Bau and M. E. Thompson, *J. Am. Chem. Soc.*, 2003, **125**, 7377–7387.
45 S. Baluschev, T. Miteva, V. Yakutkin, G. Nelles, A. Yasuda and G. Wegner, *Phys. Rev. Lett.*, 2006, **97**, 143903.
46 T. N. Singh-Rachford and F. N. Castellano, *Coord. Chem. Rev.*, 2010, **254**, 2560–2573.
47 J. Zhao, S. Ji and H. Guo, *RSC Adv.*, 2011, **1**, 937–950.
48 J.-H. Kim and J.-H. Kim, *J. Am. Chem. Soc.*, 2012, **134**, 17478–17481.
49 Y. C. Simon and C. Weder, *J. Mater. Chem.*, 2012, **22**, 20817–20830.
50 V. Gray, D. Dzebo, M. Abrahamsson, B. Albinsson and K. Moth-Poulsen, *Phys. Chem. Chem. Phys.*, 2014, **16**, 10345–10352.
51 M. Wu, D. N. Congreve, M. W. B. Wilson, J. Jean, N. Geva, M. Welborn, T. Van Voorhis, V. Bulović, M. G. Bawendi and M. A. Baldo, *Nat. Photonics*, 2016, **10**, 31–34.
52 S. Wieghold, A. S. Bieber, Z. A. VanOrman, L. Daley, M. Leger, J.-P. Correa-Baena and L. Nienhaus, *Matter*, 2019, **1**, 705–719.
53 P. Bharmoria, H. Bildirir and K. Moth-Poulsen, *Chem. Soc. Rev.*, 2020, **49**, 6529–6554.
54 J. Alves, J. Feng, L. Nienhaus and T. W. Schmidt, *J. Mater. Chem. C*, 2022, **10**, 7783–7798.
55 A. Ronchi and A. Monguzzi, *Chem. Phys. Rev.*, 2022, **3**, 041301.
56 M. Uji, T. J. B. Zähringer, C. Kerzig and N. Yanai, *Angew. Chem., Int. Ed.*, 2023, **62**, e202301506.
57 K. Wang, R. P. Cline, J. Schwan, J. M. Strain, S. T. Roberts, L. Mangolini, J. D. Eaves and M. L. Tang, *Nat. Chem.*, 2023, **15**, 1172–1178.
58 T. Mizokuro, A. Abulikemu, K. Suzuki, Y. Sakagami, R. Nishii, T. Jin and K. Kamada, *Phys. Chem. Chem. Phys.*, 2020, **22**, 17807–17813.
59 B. D. Ravetz, A. B. Pun, E. M. Churchill, D. N. Congreve, T. Rovis and L. M. Campos, *Nature*, 2019, **565**, 343–346.
60 Y. Sasaki, M. Oshikawa, P. Bharmoria, H. Kouno, A. Hayashi-Takagi, M. Sato, I. Ajioka, N. Yanai and N. Kimizuka, *Angew. Chem., Int. Ed.*, 2019, **58**, 17827–17833.
61 B. Pfund, D. M. Steffen, M. R. Schreier, M.-S. Bertrams, C. Ye, K. Börjesson, O. S. Wenger and C. Kerzig, *J. Am. Chem. Soc.*, 2020, **142**, 10468–10476.
62 L. Huang, T. Le, K. Huang and G. Han, *Nat. Commun.*, 2021, **12**, 1898.
63 S. N. Sanders, T. H. Schloemer, M. K. Gangishetty, D. Anderson, M. Seitz, A. O. Gallegos, R. C. Stokes and D. N. Congreve, *Nature*, 2022, **604**, 474–478.
64 D. K. Limberg, J.-H. Kang and R. C. Hayward, *J. Am. Chem. Soc.*, 2022, **144**, 5226–5232.
65 A. Monguzzi, J. Mezyk, F. Scotognella, R. Tubino and F. Meinardi, *Phys. Rev. B: Condens. Matter Mater. Phys.*, 2008, **78**, 195112.
66 Y. Y. Cheng, T. Khoury, R. G. C. R. Clady, M. J. Y. Tayebjee, N. J. Ekins-Daukes, M. J. Crossley and T. W. Schmidt, *Phys. Chem. Chem. Phys.*, 2010, **12**, 66–71.
67 A. Haefele, J. Blumhoff, R. S. Khnayzer and F. N. Castellano, *J. Phys. Chem. Lett.*, 2012, **3**, 299–303.